# Synthesis of Fluorene-based Hyperbranched Polymers for Solution-Processable Blue, Green, Red, and White Light-Emitting Devices

**Hung-Min Shih, Ren-Chi Wu, Ping-I Shih, Chien-Lung Wang, Chain-Shu Hsu**

Department of Applied Chemistry, National Chiao Tung University, Hsinchu 30010, Taiwan, Republic of China
Correspondence to: C.-S. Hsu (E-mail: cshsu@mail.nctu.edu.tw)

Received 16 September 2011; accepted 20 October 2011; published online 19 November 2011
**DOI: 10.1002/pola.25080**

**ABSTRACT**: For the purpose of making hyperbranched polymer (Hb-Ps)-based red, green, blue, and white polymer light-emitting diodes (PLEDs), three Hb-Ps **Hb-**terfluorene (**Hb-TF**), **Hb-**4,7-bis(9,9′-dioctylfluoren-2-yl)-2,1,3-benzothiodiazole (**Hb-BFBT**), and **Hb-**4,7-bis[(9,9′-dioctylfluoren-2-yl)-thien-2-yl]-2,1,3-benzothiodiazole (**Hb-BFTBT**) were synthesized via [2+2+2] polycyclotrimerization of the corresponding diacetylene-functionalized monomers. All the synthesized polymers showed excellent thermal stability with degradation temperature higher than 355 °C and glass transition temperatures higher than 50 °C. Photoluminance (PL) and electroluminance (EL) spectra of the polymers indicate that **Hb-TF**, **Hb-BFBT**, and **Hb-BFTBT** are blue-green, green, and red emitting materials. Maximum brightness of the double-layer devices of **Hb-TF**, **Hb-BFBT**, and **Hb-BFTBT** with the device configuration of indium tin oxide/poly(3,4-ethylene dioxythiophene):poly(styrene sulfonate)/light-emitting polymer/CsF/Al are 48, 42, and 29 cd/m$^2$; the maximum luminance efficiency of the devices are 0.01, 0.02, and 0.01 cd/A. By using host–guest doped system, saturated red electrophosphorescent devices with a maximum luminance efficiency of 1.61 cd/A were obtained when **Hb-TF** was used as a host material doped with Os(fptz)$_2$(PPh$_2$Me$_2$)$_2$ as a guest material. A maximum luminance efficiency of 3.39 cd/A of a red polymer light-emitting device was also reached when **Hb-BFTBT** was used as the guest in the PFO (Poly(9,9-dioctylfluorene)) host layer. In addition, a series of efficient white devices were, which show low turn-on voltage (3.5 V) with highest luminance efficiency of 4.98 cd/A, maximum brightness of 1185 cd/m$^2$, and the Commission Internationale de l'Eclairage (CIE) coordinates close to ideal white emission (0.33, 0.33), were prepared by using BFBT as auxiliary dopant. © 2011 Wiley Periodicals, Inc. J Polym Sci Part A: Polym Chem 50: 696–710, 2012

**KEYWORDS**: electrophosphorescent devices; host materials; hyperbranched polymers; polymer light-emitting diodes; polyfluorene

**INTRODUCTION** Polymer light-emitting diodes (PLEDs) have been attracting great interest because of their potential applications in full-color flat panel displays and in solid-state lighting.[1–3] Display and lighting applications require the development of highly efficient red, green, and blue light-emitting materials with high stability and purity.[4] Polyfluorene (PF) is the most promising blue-light emitter for PLED application because of its high photoluminescence (PL) quantum efficiency and good chemical and thermal stability.[5–9] To be used in full-color displays and lighting applications, the emission spectra of PF-based polymers have been turned to cover the entire visible region by incorporating electron-deficient monomer into the PF backbone or by physically doping with fluorescent and phosphorescent dyes with green or red emission.[10–12] Several electron-deficient monomers have been reported as the comonomers to be incorporated into the polymer backbone of wide band gap polymers. For example, Jen and coworkers[10] demonstrated efficient green emitting polymers synthesized from copolymerization of fluorene with an electron-deficient monomer, 2,1,3-benzothiadiazole (BT). Recently, Cao and coworkers[11] report a series of fluorene and 4,7-dithienyl-BT (DTBT) copolymers.[11] Devices based on the copolymers emitted a saturated red light, with $\lambda_{max}$ ranging from 628 to 674 nm. In these cases, the narrow band gap unit functioned as an exciton trap, which allowed intramolecular energy transfer from the fluorene segment to the BT or DTBT units; exciton emission was centered on the BT and DTBT units and resulted in green and red emission. Based on the concept, Shu et al. developed a series of single white light-emitting copolymers, which contain fluorene, BT, and red DTBT moieties in their polymer backbones. By controlling the feed ratio of BT and DTBT, the resulting copolymers emit white light, with contributions from all three primary colors.[12] Although the studies demonstrated the success in modifying emission colors of PF-based polymers, the control of color stability among different batches of the

polymers is relatively difficult, because the emission colors of these polymers are also dependent on the molecular weights ($M_w$) and the actual molar ratio of the electron-deficient moieties in the polymers, which is not readily controllable.

In these regards, monodisperse luminescent oligomers characterized with well-defined molecular structures and $M_w$s are developed.[13] For example, Wong et al. demonstrated a series of terfluorene (TF) and oligofluorene oligomers that show bipolar transport properties with $\lambda_{max}$ of PL at around 427 nm. These oligomers are used as efficient blue emitters and good host materials in the highly bright-blue organic light-emitting diodes (OLEDs) devices.[14–16] Wong et al. also synthesized a highly efficient green emitter (PL, $\lambda_{max}$: 544 nm) by incorporating the BT units into the oligoflourenes. The resulting molecules exhibit excellent solid-state PL quantum yields.[17] Chen and coworkers[18] further incorporated various electron-deficient segments into molecular structure of oligofluorenes to obtain a series of green and red emitting oligomers.

Hyperbranched polymers (Hb-Ps) have been widely studied in the past decades because of their unique molecular architectures and specific properties.[19–27] Because of their unique architectures, Hb-Ps have been widely reported as chemical sensors, drug delivery carriers, molecular antennae, and immunodiagnostic probes.[28–34] Recently, Tang and coworkers[35–37] developed a facial approach to synthesize conjugated Hb-polyarylenes (Hb-PAs) through the diyne [2+2+2] polycyclotrimerizations, catalyzed by transition metal complexes. Their Hb-PAs are spin coated through solution processing and show excellent optical properties, such as high light-emitting efficiency and superb optical-limiting performance.[38–42]

To combine the advantageous color stability and purity of oligomeric light-emitting molecules, and the convenience and low cost of the solution processes, in this article, we developed a facile approach to synthesize blue, green, and red emitting Hb-Ps, that is, **Hb-TF**, **Hb-**4,7-bis(9,9′-dioctylfluoren-2-yl)-2,1,3-benzothiodiazole (**BFBT**), and **Hb-**4,7-bis[(9,9′-dioctylfluoren-2-yl)-thien-2-yl]-2,1,3-benzothiodiazole (**BFTBT)** through the [2+2+2] polycyclotrimerization (Scheme 4). As illustrated in Scheme 4, we first synthesized TF, BFBT, and BFTBT as the blue, green, and red chromophores and modified them into diyne-functionalized monomers, **M1**, **M2**, and **M3**. [2+2+2] polycyclotrimerization was then introduced to convert the acetylene groups of the monomers into benzene rings, which act as the branching points in the resulting Hb-Ps. As the branch points limit the extension of the conjugation length of the repeating units, the concept retains the advantage of color stability of oligomeric analogs and enable solution processability of the resulting materials. The PL and electroluminance (EL) spectra show that **Hb-TF**, **Hb-BFBT**, and **Hb-BFTBT** are solution-processable blue, green, and red emitters. **Hb-TF** was further used as host material because of its large $E_g$. Red electrophosphorescent devices were fabricated by using **Hb-TF** as a host and a red-emitting osmium complex as a guest in the emitting layer, which demonstrate the potential of **Hb-TF** as a host material.[43] The device efficiency of the red emitter, **Hb-BFTBT**, was further improved in a host–guest doped system, where **Hb-BFTBT** was used as red-emitting guest in the PFO host layer. Furthermore, by adding BFBT, as auxiliary dopant in the PFO:**Hb-BFTBT** blend, white PLEDs with Commission Internationale de l'Eclairage (CIE) coordinates (0.33, 0.37), which are close to that of ideal white light (0.33,0.33), low turn-on voltage (3.5 V) with highest luminance efficiency of 4.98 cd/A, and maximum brightness of 1185 cd/m$^2$ were also achieved.[44–46]

## EXPERIMENTAL

### Materials

Tetrahydrofuran (THF) was distilled over sodium under nitrogen. Toluene was dried over calcium hydride and then distilled under nitrogen. Triethylamine ($Et_3N$) was dried over potassium hydroxide and then distilled under nitrogen. All other solvents and reagents were purchased from commercial sources and used without further purification. Compounds **1**, **2**, **6**, **10**, and **13** were prepared according to reported procedures.[47] $Os(fptz)_2(PPh_2Me_2)_2$ (fptz = 3-trifluoromethyl-5-pyridyl-1,2,4-triazole) was prepared according to reported procedures.[48]

### 9,9,9′,9′,9″,9″-Hexaoctylterfluorene (3)

Compounds **1** (2.53 g, 4.90 mmol) and **2** (5.0 g, 9.80 mmol) were mixed with $Pd(PPh_3)_4$ (0.011 g, 9.8 $\mu$mol), Aliquat 336 (0.6 g, 1.25 mmol), and aqueous $K_2CO_3$ (2 M, 17 mL) in degassed toluene (60 mL). The reaction mixture was stirred at 110 °C under nitrogen for 24 h. After cooling to room temperature, the solution was poured into 50 mL of water and extracted with ethyl acetate. The combined organic layers were dried over anhydrous $MgSO_4$, and the solvent was removed under reduced pressure. The crude product was purified by column chromatography (silica gel, hexane was used as eluent) to yield 5.0 g (92%) white crystals, mp: 53 °C.

$^1$H NMR ($CDCl_3$): $\delta$ = 0.72–0.85 (m, 18H, —$(CH_2)_7$—$CH_3$), 0.98–1.11 (m, 72H, —$(CH_2)$—$(CH_2)_6$—$CH_3$), 2.00–2.01 (m, 12H, $(CH_2)$ —$(CH_2)_6$—$CH_3$), 7.25–7.35 (m, six aromatic protons), 7.72–7.90 (m, 14 aromatic protons). $^{13}$C NMR ($CDCl_3$): $\delta$ = 152.01, 151.70, 151.24, 141.03, 140.72, 127.02, 126.35, 123.18, 121.72, 120.17, 55.40, 40.60, 32.01, 30.26, 26.42, 24.04, 22.82, 14.29. MS (FAB, observed $m/z$): 1168.

### 7,7′-Dibromo-9,9,9′,9′,9″,9″-hexaoctylterfluorene (4)

A solution of compound **3** (7.5 g, 6.43 mmol) and $FeCl_3$ (0.036 g, 0.22 mmol) in $CHCl_3$ (60 mL) was stirred at room temperature. Bromine (2.24 g, 14.15 mmol) in $CHCl_3$ (10 mL) was added slowly. The reaction mixture was stirred at room temperature for 12 h and then poured into sodium thiosulfate solution (30 mL) until the red color of bromine disappeared. The solution was extracted with ethyl acetate. The combined organic layers were dried over anhydrous $MgSO_4$, and the solvent was removed under reduced pressure. The crude product was purified by column chromatography

(silica gel, hexane was used as eluent) to yield 7.2 g (85%) white solid, mp: 50 °C.

$^1$H NMR ($CDCl_3$): $\delta$ = 0.72–0.85 (m, 18H, —$(CH_2)_7$—$\underline{CH_3}$), 0.98–1.11 (m, 72H, —$(CH_2)$—$(\underline{CH_2})_6$—$CH_3$), 2.00–2.01 (m, 12H, $(\underline{CH_2})$—$(CH_2)_6$—$CH_3$), 7.33–7.35 (m, two aromatic protons), 7.49 (d, two aromatic protons), 7.58–7.66 (m, 10 aromatic protons), 7.73–7.83 (m, 4 aromatic protons). $^{13}$C NMR ($CDCl_3$): $\delta$ = 153.47, 151.99, 151.70, 151.22, 141.01, 140.69, 140.53, 139.43, 127.20, 127.00, 126.38, 126.25, 123.16, 121.62, 121.30, 120.01, 119.94, 55.40, 40.60, 32.01, 30.26, 26.42, 24.04, 22.82, 14.29. MS (FAB, observed *m*/*z*): 1322.

### 7,7′-Bis(trimethylsilylethynyl)-9,9,9′,9′,9″,9″-hexaoctylterfluorene (5)

A mixture of compound **4** (7.0 g, 5.29 mmol), $PdCl_2(PPh_3)_2$ (0.075 g, 0.11 mmol), CuI (0.08 g, 0.42 mmol), and $PPh_3$ (0.11 g, 0.42 mmol) in $Et_3N$ (150 mL) was stirred at 85 °C under nitrogen. Trimethylsilyl acetylene (2.1 g, 21.18 mmol) was added slowly. The reaction mixture was allowed to react at 85 °C under nitrogen for 12 h. After cooling to room temperature, the solution was poured into $NH_4Cl$ aqueous solution and extracted with ethyl acetate. The combined organic layers were dried over anhydrous $MgSO_4$, and the solvent was removed under reduced pressure. The crude product was purified by column chromatography (silica gel, hexane was used as eluent) to yield 3.0 g (42%) white crystals, mp: 42 °C.

$^1$H NMR ($CDCl_3$): $\delta$ = 0.305 (s, 18H, —$\underline{CH_3}$), 0.68–0.85 (m, 18H, —$(CH_2)_7$—$\underline{CH_3}$), 1.08–1.19 (m, 72H, —$(CH_2)$—$(\underline{CH_2})_6$—$CH_3$), 2.00–2.06 (m, 12H, $(\underline{CH_2})$—$(CH_2)_6$—$CH_3$), 7.47–7.50 (m, four aromatic protons), 7.61–7.68 (m, 10 aromatic protons), 7.75–7.83 (m, four aromatic protons). $^{13}$C NMR ($CDCl_3$): $\delta$ = 152.04, 151.12, 141.22, 140.56, 139.80, 126.42, 121.60, 120.51, 106.52, 55.40, 40.60, 32.01, 30.26, 26.42, 24.04, 22.82, 14.29. MS (FAB, observed *m*/*z*): 1359.

### 7,7′-Diethynyl-9,9,9′,9′,9″,9″-hexaoctylterfluorene (M1)

A mixture of compound **5** (1.5 g, 5.42 mmol) and $K_2CO_3$ (0.5 g, 27.08 mmol) in MeOH/THF (6 mL, v/v = 1/3) was stirred at room temperature for 12 h. After cooling to room temperature, the solution was poured into 50 mL of water and extracted with ethyl acetate. The combined organic layers were dried over anhydrous $MgSO_4$, and the solvent was removed under reduced pressure. The crude product was purified by column chromatography (silica gel, hexane was used as eluent) to yield 1.1 g (82%) yellow oil.

$^1$H NMR ($CDCl_3$): $\delta$ = 0.68–0.85 (m, 18H, —$(CH_2)_7$—$\underline{CH_3}$), 1.08–1.19 (m, 72H, —$(CH_2)$—$(\underline{CH_2})_6$—$CH_3$), 2.00–2.06 (m, 12H, $(\underline{CH_2})$—$(CH_2)_6$—$CH_3$), 3.17 (s, 2H, ≡C—$\underline{H}$), 7.51–7.54 (m, four aromatic protons), 7.64–7.70 (m, 10 aromatic protons), 7.78–7.85 (m, four aromatic protons). $^{13}$C NMR ($CDCl_3$): $\delta$ = 152.06, 151.12, 141.22, 140.56, 139.80, 126.42, 121.60, 120.51, 106.52, 84.5, 55.40, 40.60, 32.01, 30.26, 26.42, 24.04, 22.82, 14.29. MS (FAB, observed *m*/*z*): 1214.

### 4,7-Bis(9,9′-dioctylfluoren-2-yl)-2,1,3-benzothiodiazole (7)

Compounds **6** (1.00 g, 3.40 mmol) and **2** (3.86 g, 7.48 mmol) were mixed with $Pd(PPh_3)_4$ (0.008 g, 0.0034 mmol), Aliquat 336 (0.22 g, 0.85 mmol), and aqueous $K_2CO_3$ (2 M, 14 mL) in degassed toluene (40 mL). The reaction mixture was stirred at 110 °C under nitrogen for 24 h. After cooling to room temperature, the solution was poured into 50 mL of water and extracted with ethyl acetate. The combined organic layers were dried over anhydrous $MgSO_4$, and the solvent was removed under reduced pressure. The crude product was purified by column chromatography (silica gel, ethyl acetate/hexane = 1/50 was used as eluent) to yield 3.0 g (96%) yellow oil.

$^1$H NMR ($CDCl_3$): $\delta$ = 0.72 (m, 12H, —$(CH_2)_7$—$\underline{CH_3}$), 0.98–1.11 (m, 48H, —$(CH_2)$—$(\underline{CH_2})_6$—$CH_3$), 2.00–2.05 (m, 8H, $(\underline{CH_2})$—$(CH_2)_6$—$CH_3$), 7.31–7.41 (m, six aromatic protons), 7.76–8.05 (m, 10 aromatic protons). $^{13}$C NMR ($CDCl_3$): $\delta$ = 154.58, 151.54, 151.35, 141.55, 140.88, 136.40, 133.82, 128.36, 128.12, 127.48, 127.06, 124.10, 123.18, 120.17, 119.92, 55.40, 40.60, 32.01, 30.26, 26.42, 24.04, 22.82, 14.29. MS (FAB, observed *m*/*z*): 913.

### 4,7-Bis(7-bromo-9,9′-dioctylfluoren-2-yl)-2,1,3-benzothiodiazole (8)

A solution of compound **7** (3.4 g, 3.72 mmol) and $FeCl_3$ (0.030 g, 0.19 mmol) in $CHCl_3$ (40 mL) was stirred at room temperature. Bromine (1.3 g, 8.22 mmol) in $CHCl_3$ (10 mL) was added slowly. The reaction mixture was stirred at room temperature for 12 h and then poured into sodium thiosulfate solution (20 mL) until the red color of bromine disappeared. The solution was extracted with ethyl acetate. The combined organic layers were dried over anhydrous $MgSO_4$, and the solvent was removed under reduced pressure. The crude product was purified by recrystallization from THF/MeOH (v/v = 1/3) to yield 2.9 g (73%) green crystals, mp: 40 °C.

$^1$H NMR ($CDCl_3$): $\delta$ = 0.72 (m, 12H, —$(CH_2)_7$—$\underline{CH_3}$), 0.98–1.11 (m, 48H, —$(CH_2)$—$(\underline{CH_2})_6$—$CH_3$), 2.00–2.05 (m, 8H, $(\underline{CH_2})$—$(CH_2)_6$—$CH_3$), 7.47–7.51 (d, four aromatic protons), 7.61–7.65 (d, two aromatic protons), 7.82–8.04 (m, eight aromatic protons). $^{13}$C NMR ($CDCl_3$): $\delta$ = 154.51, 153.77, 151.36, 140.85, 140.48, 139.89, 136.83, 136.33, 134.02, 133.75, 130.31, 128.57, 128.20, 126.50, 124.15, 123.20, 121.53, 120.05, 55.40, 40.60, 32.01, 30.26, 26.42, 24.04, 22.82, 14.29. MS (FAB, observed *m*/*z*): 1071.

### 4,7-Bis(7-(3-hydroxy-3-methylbut-1-ynyl)-9,9′-dioctylfluoren-2-yl)-2,1,3-benzothiodiazole (9)

A mixture of compound **8** (2.4 g, 2.24 mmol), $PdCl_2(PPh_3)_2$ (0.22 g, 0.31 mmol), CuI (0.051 g, 0.27 mmol), and $PPh_3$ (0.12 g, 0.46 mmol) in $Et_3N$ (50 mL) was stirred at 85 °C under nitrogen. 2-Methylbut-3-yn-2-ol (1.13 g, 13.43 mmol) was added slowly. The resulting solution was allowed to react at 85 °C under nitrogen for 12 h. After cooling to room temperature, the solution was poured into 50 mL of $NH_4Cl$ aqueous solution and extracted with ethyl acetate. The combined organic layers were dried over anhydrous $MgSO_4$, and the solvent was removed under reduced pressure. The crude product was purified by column chromatography (silica gel, ethyl acetate/hexane = 1/5 was used as eluent) to yield 2.21 g (91%) yellow crystals, mp: 70 °C.

$^1$H NMR ($CDCl_3$): $\delta$ = 0.72 (m, 12H, —$(CH_2)_7$—$CH_3$), 0.98–1.11 (m, 48H, —$(CH_2)$—$(CH_2)_6$—$CH_3$), 1.67 (s, 12H, —C—(OH)—$(CH_3)_2$), 2.00–2.05 (m, 10H, $(CH_2)$ —$(CH_2)_6$—$CH_3$—OH), 7.43–7.46 (d, four aromatic protons), 7.69–7.72 (d, two aromatic protons), 7.83–7.87 (d, two aromatic protons), 7.88 (s, two aromatic protons), 7.94 (s, two aromatic protons), 8.02–8.04 (d, two aromatic protons). $^{13}$C NMR ($CDCl_3$): $\delta$ = 154.52, 151.56, 141.14, 140.82, 136.84, 133.75, 131.00, 128.52, 128.16, 126.35, 124.12, 121.36, 120.25, 120.04, 94.00, 83.36, 66.02, 55.40, 40.60, 32.01, 30.26, 26.42, 24.04, 22.82, 14.29. MS (FAB, observed *m*/*z*): 1077.

### 4,7-Bis(7-ethynyl-9,9′-dioctylfluoren-2-yl)-2,1,3-benzothiodiazole (M2)

A mixture of KOH (2.08 g, 27.08 mmol) and compound **9** (2.0 g, 5.42 mmol) in toluene (40 mL) was stirred at 110 °C under nitrogen for 12 h. After cooling to room temperature, the solution was poured into 50 mL of water and extracted with ethyl acetate. The combined organic layers were dried over anhydrous $MgSO_4$, and the solvent was removed under reduced pressure. The crude product was purified by column chromatography (silica gel, ethyl acetate/hexane = 1/6 was used as eluent) to yield 1.8 g (95%) yellow oil.

$^1$H NMR ($CDCl_3$): $\delta$ = 0.72–0.90 (m, 12H, —$(CH_2)_7$—$CH_3$), 0.98–1.11 (m, 48H, —$(CH_2)$—$(CH_2)_6$—$CH_3$), 2.00–2.05 (m, 8H, $(CH_2)$—$(CH_2)_6$—$CH_3$—OH), 3.17 (s, 2H, ≡ C—H), 7.51–7.54 (d, four aromatic protons), 7.71–7.74 (d, two aromatic protons), 7.75–7.89 (m, four aromatic protons), 7.95 (s, two aromatic protons), 8.02–8.03 (d, two aromatic protons). $^{13}$C NMR ($CDCl_3$): $\delta$ = 154.28, 151.33, 141.42, 140.46, 139.28, 136.75, 133.52, 131.26, 128.31, 127.95, 126.61, 123.92, 120.43, 120.12, 119.85, 114.06, 84.70, 55.40, 40.60, 32.01, 30.26, 26.42, 24.04, 22.82, 14.29. MS (FAB, observed *m*/*z*): 962.

### 2-Bromo-7-(triisopropylsilylethynyl)-9,9′-dioctylfluorene (11)

A mixture of compound **10** (4.0 g, 7.43 mmol), $PdCl_2(PPh_3)_2$ (0.52 g, 0.74 mmol), and CuI (0.028 g, 0.15 mmol) in piperidine (50 mL) was stirred at 40 °C under nitrogen. Ethynyltriisopropylsilane (1.50 g, 8.20 mmol) was added slowly. The resulting solution was allowed to react at 40 °C under nitrogen for 12 h. After cooling to room temperature, the solution was poured into 50 mL of $NH_4Cl$ aqueous solution and extracted with ethyl acetate. The combined organic layers were dried over anhydrous $MgSO_4$, and the solvent was removed under reduced pressure. The crude product was purified by column chromatography (silica gel, hexane was used as eluent) to yield 3.50 g (92%) yellow crystals.

$^1$H NMR ($CDCl_3$): $\delta$ = 0.80 (t, $J$ = 6.90 Hz, 6H, —$(CH_2)_7$—$CH_3$), 1.01–1.23 (m, 24H, —$(CH_2)$—$(CH_2)_6$—$CH_3$), 1.64 (s, 12H, —$C(CH_3)_2$—OH), 1.90 (t, 4H, —$(CH_2)$—$(CH_2)_6$—$CH_3$), 2.11 (s, 2H, —$C(CH_3)_2$—OH), 7.37 (d, two aromatic protons), 7.51 (s, two aromatic protons), 7.57 (d, two aromatic protons). $^{13}$C NMR ($CDCl_3$): $\delta$ = 151.34, 141.02, 131.15, 126.43, 121.77, 120.22, 94.28, 83.42, 66.17, 55.58, 40.75, 40.72, 32.18, 31.96, 30.38, 29.63, 24.04, 22.99, 14.48. MS (EI, observed *m*/*z*): 592.

### 2-(4,4,5,5-Tetramethyl-1,3,2-dioxaborolan-2-yl)-7-(triisopropylsilylethynyl)-9,9′-dioctylfluorene (12)

*n*-Butyllithium (5.4 mL, 10.64 mmol, 2.5 M solution in hexane) was added into a solution of compound **11** (3.5 g, 5.9 mmol) in anhydrous THF (100 mL), which was cooled to −78 °C, and the obtained solution was stirred for 2 h, and then 2-isopropoxy-4,4,5,5-tetramethyl-1,3,2-dioxaborolane (3.8 mL, 14.75 mmol) was added slowly. The reaction mixture was warmed up slowly to room temperature and then stirred for 12 h. The mixture was quenched with water and extracted with ethyl acetate. The combined organic layers were dried over anhydrous $MgSO_4$, and the solvent was removed under reduced pressure. The crude product was purified by column chromatography (silica gel, hexane was used as eluent) to yield 2.7 g (52%) white solid, mp: 25 °C.

$^1$H NMR ($CDCl_3$): $\delta$ = 0.72 (t, 6H, —$(CH_2)_7$—$CH_3$), 0.98–1.11 (m, 24H, —$(CH_2)$—$(CH_2)_6$—$CH_3$), 1.39 (s, 12H, —$CH_3$), 1.98 (t, 4H, $(CH_2)$—$(CH_2)_6$—$CH_3$), 7.25–7.35 (m, three aromatic protons), 7.70–7.80 (m, four aromatic protons). $^{13}$C NMR ($CDCl_3$): $\delta$ = 151.54, 150.09, 144.36, 141.14, 133.93, 129.05, 127.71, 126.88, 123.15, 120.31, 119.18, 83.92, 55.30, 40.49, 32.02, 30.23, 29.43, 25.17, 23.89, 22.82, 14.31. MS (EI, observed *m*/*z*): 640.

### 4,7-Bis(5-(7-(triisopropylsilylethynyl)-9,9′-dioctylfluoren-2-yl)-thien-2-yl)-2,1,3-benzothiodiazole (14)

Compounds **13** (0.77 g, 1.70 mmol) and **12** (2.70 g, 4.20 mmol) were mixed with $Pd_2(dba)_3$ (0.05 g, 0.05 mmol), Aliquat 336 (0.16 g, 0.63 mmol), and aqueous $Cs_2CO_3$ (15 mL, 5.8 mmol, 0.4 M) in degassed toluene (40 mL). The reaction mixture was stirred at 110 °C under nitrogen for 24 h. After cooling to room temperature, the solution was poured into 50 mL of water and extracted with ethyl acetate. The combined organic layers were dried over anhydrous $MgSO_4$, and the solvent was removed under reduced pressure. The crude product was purified by column chromatography (silica gel, hexane was used as eluent) to yield 0.6 g (25%) red oil.

$^1$H NMR ($CDCl_3$): $\delta$ = 0.72 (t, 6H, —$(CH_2)_7$—$CH_3$), 0.98–1.11 (m, 24H, —$(CH_2)$ —$(CH_2)_6$—$CH_3$), 1.36 (s, 12H, —$CH_3$), 1.98 (t, 4H, $(CH_2)$—$(CH_2)_6$—$CH_3$), 7.25–7.35 (m, three aromatic protons), 7.60–7.82(m, four aromatic protons). MS (FAB, observed *m*/*z*): 1324.

### 4,7-Bis(5-(7-diethynyl-9,9-dioctylfluoren-2-yl)-thien-2-yl)-2,1,3-benzothiodiazole (M3)

Tetrabutylammonium fluoride (TBAF) (1.3 mL, 1.3 mmol, 1.0 M in THF) was added to a solution of compound **14** (0.60 g, 0.45 mmol) in anhydrous THF (20 mL) at room temperature, and the reaction mixture was stirred at room temperature for 1 h. The solution was poured into 50 mL of water and extracted with ethyl acetate. The combined organic layers were dried over anhydrous $MgSO_4$, and the solvent was removed under reduced pressure. The crude product was purified by column chromatography (silica gel, ethyl acetate/hexane = 1/6 was used as eluent) to give 0.45 g (90%) red oil.

$^1$H NMR ($CDCl_3$): $\delta$ = 0.67–0.90 (t, $J$ = 7.05 Hz, 6H, —$(CH_2)_7$—$CH_3$), 1.02–1.58 (m, 24H, —$(CH_2)$—$(CH_2)_6$—$CH_3$),

2.03 (t, $J$ = 3.90 Hz, 4H, —($C\underline{H}_2$)—$(CH_2)_6$—$CH_3$), 3.17 (s, 2H, ≡C—$\underline{H}$), 7.35 (d, four aromatic protons), 7.50 (d, $J$ = 7.80 Hz, four aromatic protons), 7.66 (d, four aromatic protons), 7.72 (s, two aromatic protons), 7.95 (s, two aromatic protons), 8.16 (d, two aromatic protons). $^{13}$C NMR ($CDCl_3$): $\delta$ = 150.62, 140.55, 130.81, 126.11, 120.40, 119.53, 84.09, 54.77, 39.79, 39.76, 31.32, 29.51, 29.49, 28.76, 23.21, 22.14, 13.62. MS (FAB, observed $m/z$): 1012.

### General Polymerization Procedure

The monomers were polymerized using $TaCl_5$ as the catalyst. All polymerization reactions and manipulations were carried out under nitrogen using either an inert-atmosphere glove box or Schlenk techniques in a vacuum line system. The purification of the polymers was done in a fume hood. A typical experimental procedure for the polymerization of monomer **M1** is given below as an example (Scheme 4). Monomer **1** (0.6 g, 0.49 mmol) was added into a Schlenk tube with a three-way stopcock on the sidearm. The tube was evacuated under vacuum and then flushed with dried nitrogen three times through sidearm. Dried toluene (5 mL) was injected into the tube through a septum to dissolve the monomer. The catalyst solution was prepared in another tube by dissolving $TaCl_5$ (42 mg, 0.118 mmol) in 11 mL of toluene. The monomer solution was then transferred to the catalyst solution using a hypodermic syringe. The resulting mixture was stirred at room temperature under nitrogen for 8 h, and then methanol was added to the solution. The mixture was added dropwise to methanol through a cotton filter with stirring. The polymer precipitate was allowed to stand for 1 h and was then separated by filtration, purified by several reprecipitation steps from toluene solution into methanol, and then dried in a vacuum oven to yield 0.52 g (86%) yellow solid **Hb-TF**.

### Characterization

$^1$H and $^{13}$C NMR spectra were recorded on a Varian-300 MHz spectrometer. Mass spectra were obtained using a JEOL JMS-HX 110 mass spectrometer. Gel permeation chromatography (GPC) was measured using a Viscotek GPC system equipped with a Viscotek T50A differential viscometer and a Viscotek LR125 laser referactometer. Three 10-$\mu$m columns were connected in series in order of decreasing pore size ($10^5$, $10^4$, and $10^3$ Å). Polystyrene standards were used for calibration, and THF was used as the eluent. Thermogravimetric analysis (TGA) was carried out using a Perkin Elmer Pyris 7 instrument. The thermal stabilities of the samples under nitrogen were determined by measuring their weight losses while heating at a rate of 10 °C/min. Differential scanning calorimetry (DSC) was performed on a Perkin Elmer Pyris Diamond DSC unit operated at a heating and cooling rates of 20 and 40 °C/min, respectively. The glass transition temperatures ($T_g$s) were determined from the second heating scan. UV–Vis spectra were measured using an HP 8453 spectrophotometer. PL spectra were obtained using an ARC SpectraPro-150 luminance spectrometer. Cyclic voltammetry (CV) experiments were performed using an Autolab ADC 164 electrochemical analyzer operated at a scanning rate of 50 mV/s; the supporting electrolyte was 0.1 M tetra-$n$-butylammonium tetrafluoroborate ($n$-$Bu_4NBF_4$), which was dissolved in acetonitrile. The potentials were measured against an Ag/AgCl reference electrode using ferrocene/ferrocenium ($Fc/Fc^+$) as the internal standard.

### Fabrication and Measurements of PLED

Two polymer light-emitting devices having the configuration of indium tin oxide (ITO)/poly(3,4-ethylene dioxythiophene) (PEDOT):poly(styrene sulfonate) (PEDOT:PSS) (40 nm)/light-emitting polymer (60–80 nm)/CsF (2 nm)/Al (100 nm) and ITO/PEDOT:PSS (40 nm)/light-emitting polymer (60–80 nm)/TPBI (30 nm)/LiF (1 nm)/Al (100 nm) were fabricated. The patterned ITO glass substrates were ultrasonically cleaned with detergent, deionized water, acetone, and isopropyl alcohol. The PEDOT:PSS (Baytron P VP AI4083 from H. C. Stack) was spin coated on the cleaned and UV–ozone-treated ITO substrates. The PEDOT:PSS layer was baked at 120 °C for 30 min in air to remove residual water and then moved into a glove box under nitrogen. The light-emitting polymers dissolved in chlorobenzene solution were spin coated on top of the PEDOT:PSS layer. Then, the films were baked at 80 °C for 30 min under vacuum. The TPBI (1,3,5-tris(1-phenyl-1H-benzimidazol-2-ol)benzene) layer, which was grown through thermal deposition, was used as an electron transporting layer that would block holes and confine excitons. The devices were completed by thermal deposition of a CsF (2 nm)/Al (100 nm) or LiF (1 nm)/Al (100 nm) as cathode. The current–voltage–luminance characteristics were measured by using an optical power meter PR-650 and a digital source meter Keithley 2400. The EL spectra were measured by using a Photo Research PR-650 spectrophotometer under ambient condition after encapsulation.

## RESULTS AND DISCUSSION

### Synthesis and Characterization of Monomers and Polymers

Schemes 1–3 illustrate the synthetic routes of the monomers. **M1**, **M2**, and **M3** were synthesized based on the following procedure. First, reacting 2,7-dibromo-9,9-dioctylfluorene (**1**) and 2-(4,4,5,5-tetramethyl-1,3,2-dioxaborolan-2-yl)-9,9-dioctylfluorene (**2**) through Suzuki coupling reaction allows the formation of compound **3**. Compound **3** was then brominated with bromide and catalytic amount of Lewis acid, $FeCl_3$, to give compound **4**. Reacting the bromo groups of compound **4** with trimethylsilylacetylene by Sonogashira coupling reaction yielded compound **5**.[49] Finally, **M1** was obtained by deprotecting the terminal acetylene groups of compound **5** under basic condition with $K_2CO_3$. **M2** was synthesized based on the following procedure. Compound **7** was also synthesized by reacting compounds **2** and **6** through Suzuki coupling reaction. Compound **7** was then brominated with bromide to give the corresponding compound **8**,[49] which was further reacted with 2-methyl-3-butyn-2-ol by Sonogashira coupling reaction to yield compound **9**. Deportecting compound **9** under basic and high temperature condition allows the formation of monomer **M2**. **M3** was synthesized based on the following procedure. Compound **14** was synthesized by reacting compounds **12** and **13** through Suzuki coupling reaction. Compound 14 was deprotect with

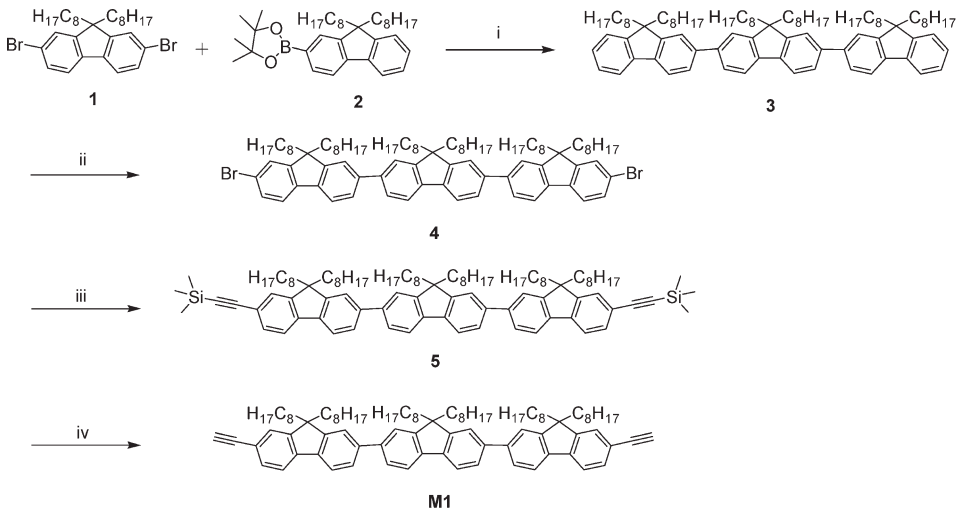


[a] Reagents and conditions: i) $Pd(PPh_3)_4$, $K_2CO_3$, Aliquat 336, toluene, $H_2O$, reflux; ii) $FeCl_3$, $Br_2$, $CHCl_3$, 0 °C; iii) Trimethylsilylacetylene, $PdCl_2(PPh_3)_2$, CuI, $PPh_3$, $Et_3N$, 85 °C; iv) $K_2CO_3$, MeOH/THF (1:3, v/v), r.t..

**SCHEME 1** Synthetic route of **M1**. Reagents and conditions: (i) $Pd(PPh_3)_4$, $K_2CO_3$, Aliquat 336, toluene, $H_2O$, reflux; (ii) $FeCl_3$, $Br_2$, $CHCl_3$, 0 °C; (iii) trimethylsilylacetylene, $PdCl_2(PPh_3)_2$, CuI, $PPh_3$, $Et_3N$, 85 °C; (iv) $K_2CO_3$, MeOH/THF (1:3, v/v), r.t.

n-$Bu_4NF$ under basic condition to allow the formation of monomer **M3**.

**M1**, **M2**, and **M3** were characterized with $^1H$ and $^{13}C$ NMR spectroscopy and FAB-MS (Supporting Information). In the $^1H$ NMR spectra, the characteristic peak of —C≡C—H at $\delta$ 3.17 ppm was observed for all of the monomers, which indicates the success of Sonogashira coupling reactions and the deprotection reactions. Compared to the $^1H$ NMR spectrum of **M1**, a characteristic singlet peak at $\delta$ 7.95 ppm that belongs to the aromatic H on the BT unit can be observed for **M2**. For monomer **M3**, the double peaks at $\delta$ 7.66 ppm represent the protons in the thiophene rings of DTBT. Thus, the $^1H$ NMR spectra differentiate the difference in the molecular structures of the monomers. In the $^{13}C$ NMR spectra, the feature signal peak of the carbon on the terminated triple bond of the monomers was also observed at $\delta$ 84.5 ppm. In the mass spectra, the $m/z$ values of 1214, 962, and 1012 were observed for **M1**, **M2**, and **M3**, which closely match

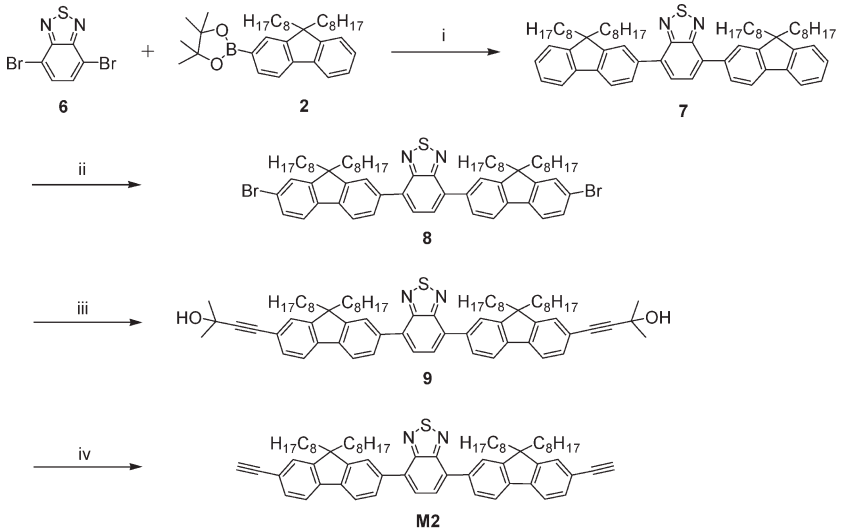


[b] Reagents and conditions: i) $Pd(PPh_3)_4$, $K_2CO_3$, Aliquat 336, toluene, $H_2O$, reflux; ii) $FeCl_3$, $Br_2$, $CHCl_3$, 0 °C; iii) 2-Methyl-3-butyn-2-ol, $PdCl_2(PPh_3)_2$, CuI, $PPh_3$, $Et_3N$, reflux; iv) KOH, toluene, reflux.

**SCHEME 2** Synthetic route of **M2**. Reagents and conditions: (i) $Pd(PPh_3)_4$, $K_2CO_3$, Aliquat 336, toluene, $H_2O$, reflux; (ii) $FeCl_3$, $Br_2$, $CHCl_3$, 0 °C; (iii) 2-methyl-3-butyn-2-ol, $PdCl_2(PPh_3)_2$, CuI, $PPh_3$, $Et_3N$, reflux; (iv) KOH, toluene, reflux.

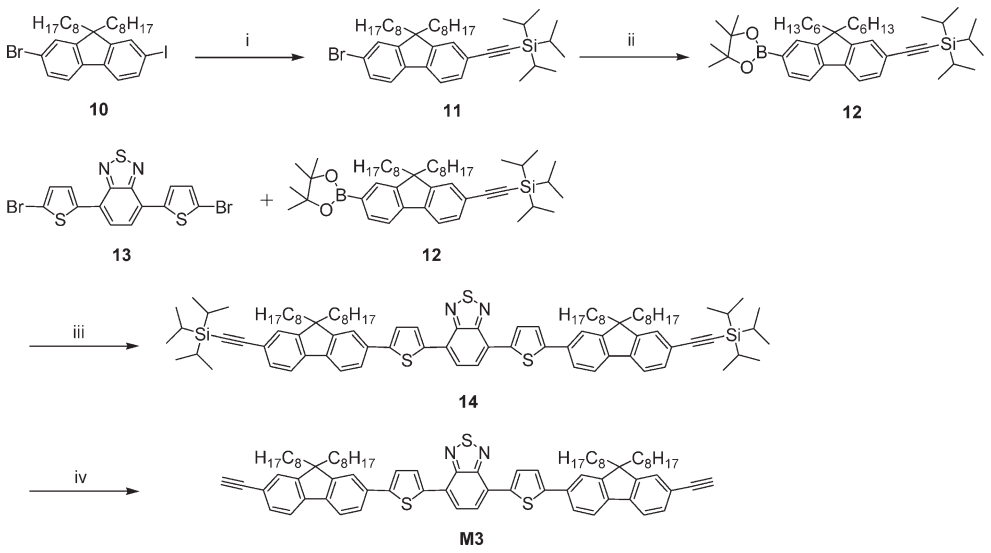


[c] Reagents and conditions: i) $PdCl_2(PPh_3)_2$, ethynyltriisopropylsilane, CuI,piperidine, 40 °C; ii) *n*-BuLi, 2-isopropyl-4,4,5,5-tetramethyl-1,3,2-dioxaborolane, THF, -78 °C; iii) $Pd(PPh_3)_4$, $K_2CO_3$, Aliquat 336, toluene, $H_2O$, reflux; iv) n-$Bu_4NF$, THF, r.t..

**SCHEME 3** Synthetic route of **M3**. Reagents and conditions: (i) $PdCl_2(PPh_3)_2$, ethynyltriisopropylsilane, CuI, piperidine, 40 °C; (ii) *n*-BuLi, 2-isopropyl-4,4,5,5-tetramethyl-1,3,2-dioxaborolane, THF, −78 °C; (iii) $Pd(PPh_3)_4$, $K_2CO_3$, Aliquat 336, toluene, $H_2O$, reflux; (iv) *n*-$Bu_4NF$, THF, r.t.

with the calculated monoisotopic masses of the monomers. All the molecular characterization results clearly indicate the success of the reactions and confirm the chemical identify of **M1**, **M2**, and **M3**. The Hb-Ps, **Hb-TF**, **Hb-BFBT**, and **Hb-BFTBT** were synthesized by using **M1**, **M2**, and **M3** as monomers via [2+2+2] polycyclotrimerization (Scheme 4). The Hb-Ps compared with the monomers show much weaker signal for the —C≡C—H proton in their $^1$H NMR spectra through the polycyclotrimerization reaction (Supporting Information Fig. S1). Thus, the peak intensities of the —C≡C—H proton ($\delta$ 3.17 ppm) decreased after the polymerization reactions, and their remaining intensities depend on the degree of polymerization. The molecular weights and polydispersity indices (PDI) of **Hb-TF**, **Hb-BFBT**, and **Hb-BFTBT** were characterized with GPC and summarized in Table 1. **Hb-TF** possesses much higher $M_w$ (136.8 × $10^3$ g/mol, PDI: 1.86) than those of **Hb-BFBT** (6.984 × $10^3$ g/mol, PDI: 1.50) and **Hb-BFTBT** (7.853 × $10^3$ g/mol, PDI: 1.43). The decomposition temperatures ($T_d$) of **Hb-TF**, **Hb-BFBT**, and **Hb-BFTBT** are 401, 355, and 400 °C, which indicate good thermal stability (Supporting Information). The polymers **Hb-TF**, **Hb-BFBT**, and **Hb-BFTBT** reveal $T_g$s at 110, 51, and 89 °C, respectively (Table 1 or Supporting Information Figs. S13–S18). It is evidenced that all the Hb-Ps show good thermal behaviors.

## Optical Properties

To examine the photophysical properties of these polymers, the absorption and PL spectra of dilute solutions and solid films **of Hb-TF**, **Hb-BFBT**, and **Hb-BFTBT** were measured. Figures 1–3 show the UV–Vis and PL spectra of the dilute solutions and thin films of **Hb-TF**, **Hb-BFBT**, and **Hb-BFTBT**, respectively. The spectral data are summarized in Table 2. In the dilute solutions, **Hb-TF** shows only one absorption band

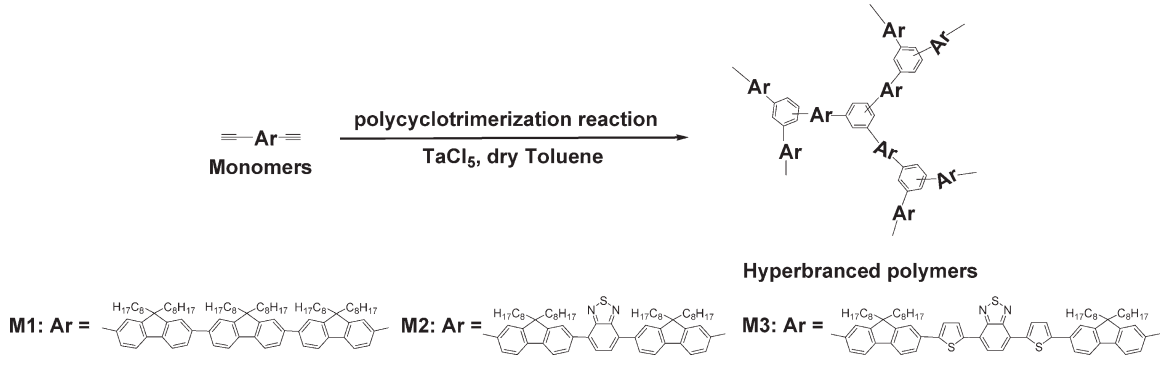


**SCHEME 4** Synthesis of **Hb-TF**, **Hb-BFBT**, and **Hb-BFTBT** from **M1**, **M2**, and **M3** by polycyclotrimerization reaction.

**TABLE 1** Number-Average Molecular Weights ($M_n$), Weight-Average Molecular Weights ($M_w$), PDI, and Thermal Properties of the Hyperbranched Polymers

| Polymer | $M_n$[a] ($\times 10^3$) | $M_w$[a] ($\times 10^3$) | PDI[a] ($M_w/M_n$) | $T_d$[b] (°C) | $T_g$[c] (°C) |
|---|---|---|---|---|---|
| **Hb-TF** | 136.8 | 255.4 | 1.86 | 401 | 110 |
| **Hb-BFBT** | 6.984 | 10.528 | 1.50 | 355 | 51 |
| **Hb-BFTBT** | 7.853 | 11.254 | 1.43 | 387 | 89 |

[a] Weight-average molecular weights ($M_w$) and PDI of the polymers were determined by GPC in THF using polystyrene standards.
[b] The 5% weight loss of the decomposition temperature measured by TGA under $N_2$.
[c] The glass transition temperature measured by DSC under $N_2$.

with $\lambda_{max}$ at 365 nm, which is originated from the localized $\pi$–$\pi^*$ transitions of the TF unit, while **Hb-BFBT** and **Hb-BFTBT** show two distinct absorption bands (Table 2). The shorter wavelength absorption bands of **Hb-BFBT** and **Hb-BFTBT** can be attributed to the localized $\pi$–$\pi^*$ transitions, and the longer wavelength absorption bands come from the intramolecular charge transfer (ICT) between electron-rich donors (fluorene) and electron-deficient acceptors (BT and DTBT).[50,51] The ICT band of **Hb-BFTBT** ($\lambda_{max}$: 527 nm) is at longer wavelength than that of **Hb-BFBT** ($\lambda_{max}$: 437 nm). The bathochromic shift was also observed in the PL $\lambda_{max}$ of the dilute solutions of **Hb-TF**, **Hb-BFBT**, and **Hb-BFTBT**. The PL $\lambda_{max}$ of **Hb-TF**, **Hb-BFBT**, and **Hb-BFTBT** are 410, 522, and 612 nm, respectively (Table 2 and Figs. 1–3). In addition, the optical band gaps ($E_g$) of the Hb-Ps deduced from the onset of absorption follows the trend that $E_{g,\ \textbf{Hb-TF}}$ (3.04 eV) $>$ $E_{g,\ \textbf{Hb-BFBT}}$ (2.45 eV) $>$ $E_{g,\ \textbf{Hb-BFTBT}}$ (1.97 eV). These results clearly indicate that the photophysical properties of the Hb-Ps are strongly affected, when the middle fluorene moiety in the TF unit is replaced with an electron-withdrawing group, for example, BT or DTBT. In addition to that, the donating strength of the fluorene moiety is stronger when the fluorene and BT moieties are bridged with a thiopene ring. The PL $\lambda_{max}$s of the polymers suggest that **Hb-TF**, **Hb-BFBT**, and **Hb-BFTBT** are blue, green, and red emitters. Thus, the results demonstrate a simple methodology for tuning the PL wavelength of hyperbranched conjugated polymers by simply introducing the electron accepting units into the electron-rich conjugated systems.

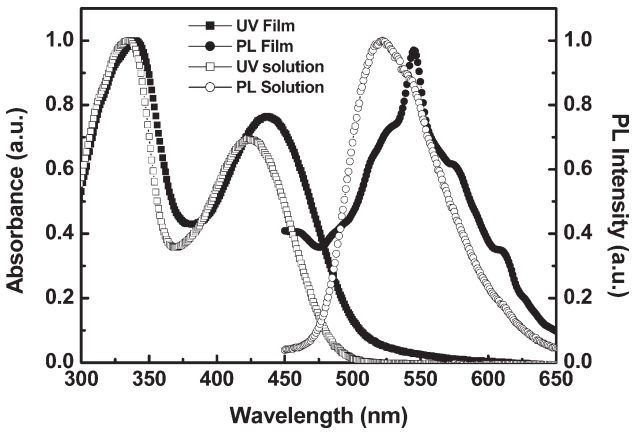


**FIGURE 2** UV–Vis absorption and PL spectra of **Hb-BFBT** in solution and in thin film.

Compared to their dilute solutions, bathochromic shift of the UV, and PL bands, decrease in the PL quantum yields are observed in the thin films of **Hb-TF**, **Hb-BFBT**, and **Hb-BFTBT** (Table 2 and Figs. 1–3). The phenomenon is attributed to the formation of aggregation of polymers in the solid state. Formation of aggregation in the solid state of these series of Hb-Ps can be expected, as the branching points (benzene rings) possess a planar geometry rather than a three-dimensional structure. Interestingly, the PL spectrum of the **Hb-TF** thin film is extremely broad and covers extensively in the blue and green light region. The result suggests the possibility of coexistence of multiple degrees of aggregations in the thin film. Although the PL spectra of the **Hb-BFBT** and **Hb-BFTBT** in thin film red-shifted, they remained green and red emitters in the solid state. Because of its large $E_g$ and wide PL emission, the thin film of **Hb-TF** therefore possesses the potential to be used as a host in PLED

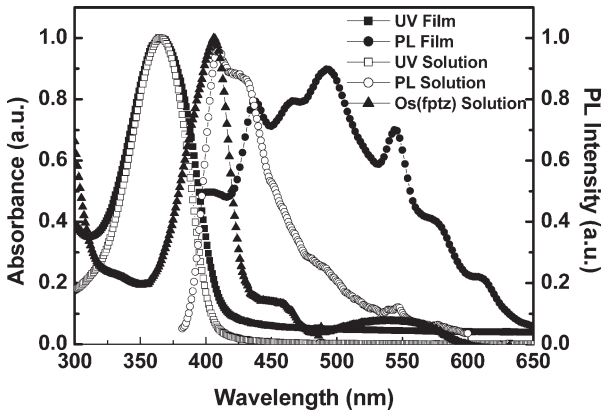


**FIGURE 1** UV–Vis absorption and PL spectra of **Hb-TF** in solution and in thin film, and the absorption spectrum of $Os(fptz)_2(PPh_2Me_2)_2$ in solution.

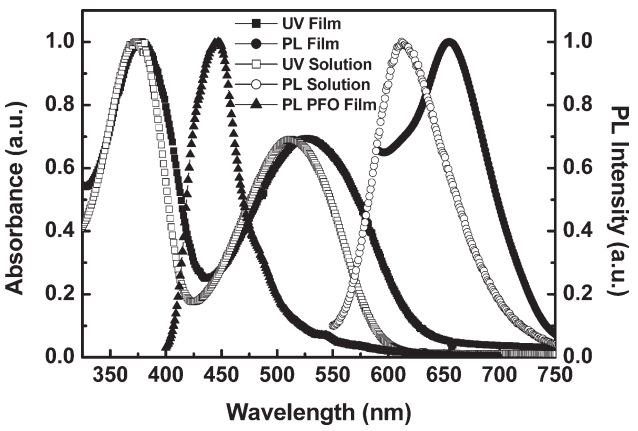


**FIGURE 3** UV–Vis absorption and PL spectra of **Hb-BFTBT** in solution and in thin film, and the PL spectrum of PFO in thin film.

**TABLE 2** Optical Properties of the Hyperbranched Polymers

| | UV–Vis Absorption $\lambda_{max}$ (nm) | | PL $\lambda_{max}$ (nm) | | $\Phi_{PL}$ (%) | | $E_g$[c] (eV) |
|---|---|---|---|---|---|---|---|
| Polymer | Solution[a] | Film[b] | Solution[a] | Film[b] | Solution[a] | Film[b] | Film[b] |
| **Hb-TF** | 365 | 366 | 410 | 438, 490, 544 | 37 | 8 | 3.04 |
| **Hb-BFBT** | 335, 423 | 340, 437 | 522 | 545 | 50 | 30 | 2.45 |
| **Hb-BFTBT** | 373, 511 | 376, 527 | 612 | 655 | 18 | 7 | 1.97 |

[a] In 0.5 wt % toluene.
[b] Spin-coated from 0.5 wt % toluene.
[c] $E_g$ was determined from the onset wavelength of UV absorption spectra in thin film.

applications or as the active layer of a white PLED when blended with suitable amount of red emitters we synthesized in this article.

### Electrochemical Properties

CV was used to examine the electrochemical properties and evaluate the HOMO (highest occupied molecular orbital) levels of the polymers. Table 3 summarizes the $E_{ox,\ onset}$, $E_{HOMO}$, and $E_{LUMO}$ (lowest unoccupied molecular orbital). **Hb-TF**, **Hb-BFBT**, and **Hb-BFTBT** exhibited oxidation onset potentials at about 1.42, 1.44, and 0.87 eV, respectively. Their $E_{HOMO}$ energy levels are calculated as –5.82, −5.84, and –5.27 eV based on the onset of oxidation potential of the internal standard ferrocene (4.8 eV below vacuum). The $E_{LUMO}$ levels of **Hb-TF**, **Hb-BFBT**, and **Hb-BFTBT** are −2.78, −3.39, and −3.30 eV, which were deduced from their $E_{HOMO}$ and optical band gaps ($E_g$). The $E_{LUMO}$ of **Hb-BFBT**, and **Hb-BFTBT** are lower than that of **Hb-TF**, because of the incorporation of BT, an electron-withdrawing group, into the conjugated system.[50] As for D-A conjugated polymers, the first oxidation onset potential is normally contributed from the electron-rich segment, the close $E_{HOMO}$ of **Hb-TF** and **Hb-BFBT** can be interpreted as the oxidation takes place first at the fluorene moieties in the molecules.[50] The higher $E_{HOMO}$ of **Hb-BFTBT** could be attributed to the incorporation of thiophene units, an electron-rich unit, into the main chain. The energy level diagrams of the polymers are illustrated in Figure 4.

### Device Performance

To evaluate the PLED performances of pristine **Hb-TF**, **Hb-BFBT**, and **Hb-BFTBT**, we fabricated the double-layer PLEDs with a device configuration of ITO/PEDOT:PSS (40 nm)/light-emitting polymer (60–80 nm)/CsF (2 nm)/Al (100 nm). The EL spectra, the current density, and brightness versus voltage characteristics of the devices are shown in Figure 5. The device performances are summarized in Table 4. As shown in Figure 5(a), the EL $\lambda_{max}$ of **Hb-TF**, **Hb-BFBT**, and **Hb-BFTBT** are located at 520, 560, and 664 nm, at maximum luminance efficiency. All the EL $\lambda_{max}$s of the devices are similar to the PL $\lambda_{max}$s observed in the polymer thin films. The EL spectrum of **Hb-TF** shows broad blue-green emission, while the EL spectra of **Hb-BFBT** and **Hb-BFTBT** refer to green and red emission. Thus, by introducing the electron-accepting units (BT and DTBT) into an electron-rich conjugated system, the emission spectra of the Hb-Ps-based devices can be easily adjusted, and RGB PLEDs can be obtained using the novel Hb-Ps as the active materials. The broad blue-green emission is due to the aggregation of the polymer chains in the solid state. The **Hb-TF**-based device had a maximum brightness of 50 cd/m$^2$ and maximum luminance efficiency of 0.01 cd/A. The **Hb-BFBT**- and **Hb-BFTBT**-based devices had a maximum brightness of 42 and 29 cd/m$^2$, and the maximum luminance efficiency of 0.02 and 0.01 cd/A, respectively. The turn-on voltage of **Hb-TF**, **Hb-BFBT**, and **Hb-BFTBT** are 7.1, 6.5, and 4.4 V, respectively (Table 4). Among these polymers, **Hb-BFTBT**-based device displayed the lowest turn-on voltage than others because of its highest $E_{HOMO}$, which reduces the energy barrier for the hole-injection from the PEDOT:PSS layer.

Because of its large $E_g$, **Hb-TF** has the potential to be used as a polymeric host. To evaluate **Hb-TF** as a host material, we used red electrophosphorescent, $Os(fptz)_2(PPh_2Me_2)_2$ as a guest material and fabricated a multilayer device with the configuration of ITO/PEDOT:PSS (40 nm)/**Hb-TF**:*X* wt % $Os(fptz)_2(PPh_2Me_2)_2$ (60–80 nm)/TPBI (30 nm)/LiF (1 nm)/Al

**TABLE 3** Electrochemical Properties of the Hyperbranched Polymers

| Polymer | $E_{ox,\ onset}$[a] (V) | $E_{HOMO}$[b] (eV) | $E_{LUMO}$[c] (eV) |
|---|---|---|---|
| **Hb-TF** | 1.42 | −5.82 | −2.78 |
| **Hb-BFBT** | 1.44 | −5.84 | −3.39 |
| **Hb-BFTBT** | 0.87 | −5.27 | −3.30 |

[a] The onset oxidation potential measured by CV.
[b] $E_{HOMO}$ is calculated based on the equation, $E_{HOMO} = -4.8 + E_{ox,\ onset}$.
[c] $E_{LUMO}$ is calculated based on the equation, $E_{LUMO} = E_g + E_{HOMO}$.

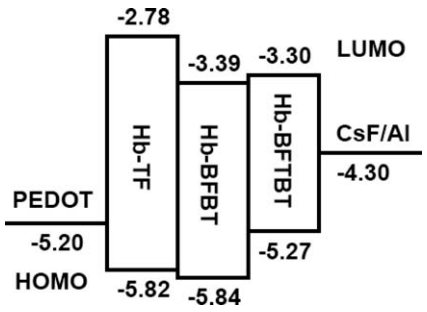


**FIGURE 4** Energy level diagram for the devices having the configuration of ITO/PEDOT:PSS/light-emitting polymer/CsF/Al.

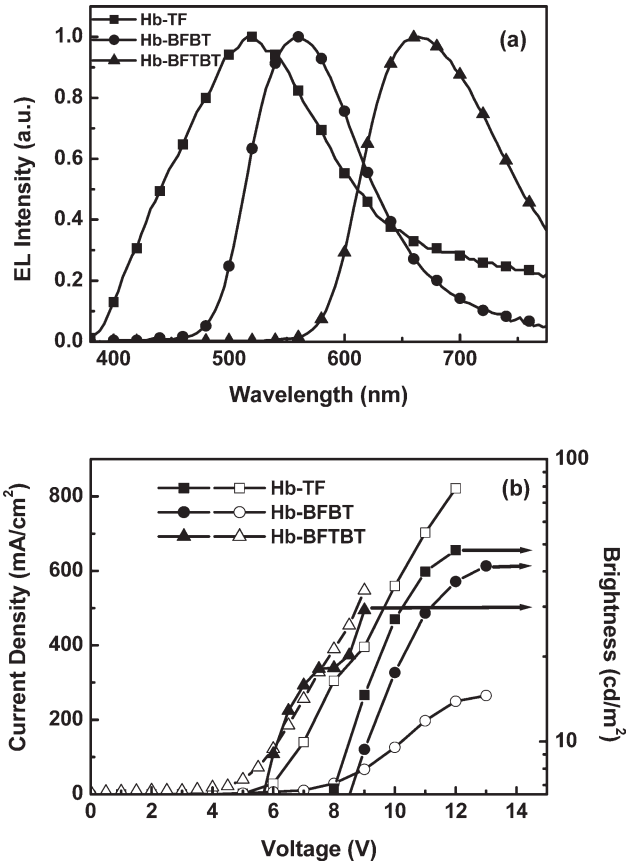


**FIGURE 5** (a) EL spectra and (b) current density and brightness versus voltage characteristics of the devices having the configuration of ITO/PEDOT:PSS/light-emitting polymer/CsF/Al.

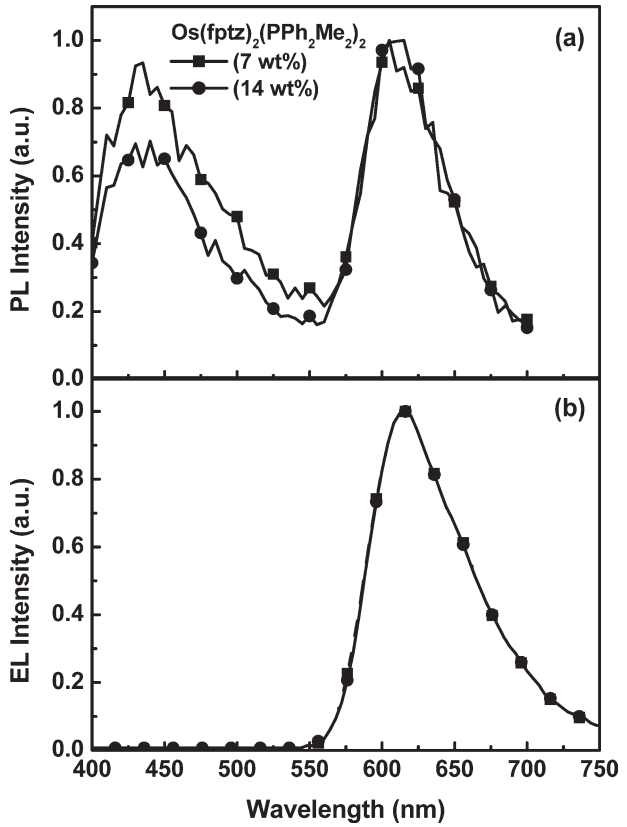


**FIGURE 6** (a) PL spectra and (b) EL spectra of the blends prepared from **Hb-TF** as the host doped with the 7 and 14 wt % of $Os(fptz)_2(PPh_2Me_2)_2$ as the guest.

(100 nm). The PL and EL spectra of 7 and 14 wt % $Os(fptz)_2(PPh_2Me_2)_2$-doped blends are presented in Figure 6. The current density and brightness versus voltage characteristics of 7 and 14 wt % $Os(fptz)_2(PPh_2Me_2)_2$-doped devices are shown in Figure 7. Device performance is summarized in Table 5. The PL spectrum of the **Hb-TF** thin film and the UV-Vis absorption spectrum of $Os(fptz)_2(PPh_2Me_2)_2$ in chlorobenzene solution shown in Figure 1 demonstrate a significant overlap between the PL band of **Hb-TF** and the metal-to-ligand charge transfer (MLCT) absorption band of $Os(fptz)_2(PPh_2Me_2)_2$. Thus, an efficient Förster energy transfer can be expected from the singlet excited state of the host to the MLCT state of the guest, $Os(fptz)_2(PPh_2Me_2)_2$. A fast intersystem crossing takes place once $Os(fptz)_2(PPh_2Me_2)_2$ is excited and subsequent red phosphorescence emission was generated when excited $Os(fptz)_2(PPh_2Me_2)_2$ relaxes from its triplet excited state.[52] As indicated in Figure 6(a), the PL spectra of the blends that contained $Os(fptz)_2(PPh_2Me_2)_2$-doped **Hb-TF** films exhibit two emission bands with $\lambda_{max}$ at 435 and 616 nm. The shorter wavelength band originates from the residual emission of the host, and the longer wavelength band corresponds to the phosphorescence of the $Os(fptz)_2(PPh_2Me_2)_2$ guest. The result implies that partial energy transfer moderated from the host to the guest. Conversely, the EL spectra of Figure 6(b) exhibited only the red emission derived from $Os(fptz)_2(PPh_2Me_2)_2$, suggesting that both energy transfer and direct charge trapping/recombination at the $Os(fptz)_2(PPh_2Me_2)_2$ guest were responsible for the observed EL.[53–55] According to the energy level diagram in inset of Figure 7(a), **Hb-TF** has much deeper HOMO level than $Os(fptz)_2(PPh_2Me_2)_2$. Therefore, holes in the active layer can be effectively trapped in the $Os(fptz)_2(PPh_2Me_2)_2$ domain. In this case, efficient charge recombination in the guest domain and dominant phosphorescence emission of the guest was observed.[56] As shown in Table 5, the EL spectra of 7 and 14 wt % $Os(fptz)_2(PPh_2Me_2)_2$-doped blends show EL $\lambda_{max}$ at 616 nm, with the CIE coordinates of (0.64, 0.36) close to the standard CIE coordinate of red emission (0.67, 0.33). Maximum brightness of the 7, and 14 wt % $Os(fptz)_2(PPh_2Me_2)_2$-doped devices are 41 and 84 cd/m$^2$, and the maximum luminance

**TABLE 4** Performances of the Devices Based on the Configuration of ITO/PEDOT:PSS/Light-Emitting Polymer/CsF/Al

| Polymer | Hb-TF | Hb-BFBT | Hb-BFTBT |
|---|---|---|---|
| Turn-on voltage (V)[a] | 7.1 | 6.5 | 4.4 |
| Max. Brightness (cd/m$^2$) | 48 @ 12 V | 42 @ 13 V | 29 @ 9 V |
| Max. L.E. (cd/A) | 0.01 | 0.02 | 0.01 |
| EL $\lambda_{max}$ (nm) | 520 | 560 | 664 |
| CIE ($x$, $y$) | (0.30, 0.39) | (0.43, 0.54) | (0.67, 0.32) |

[a] Recorded at 1 cd/m$^2$.

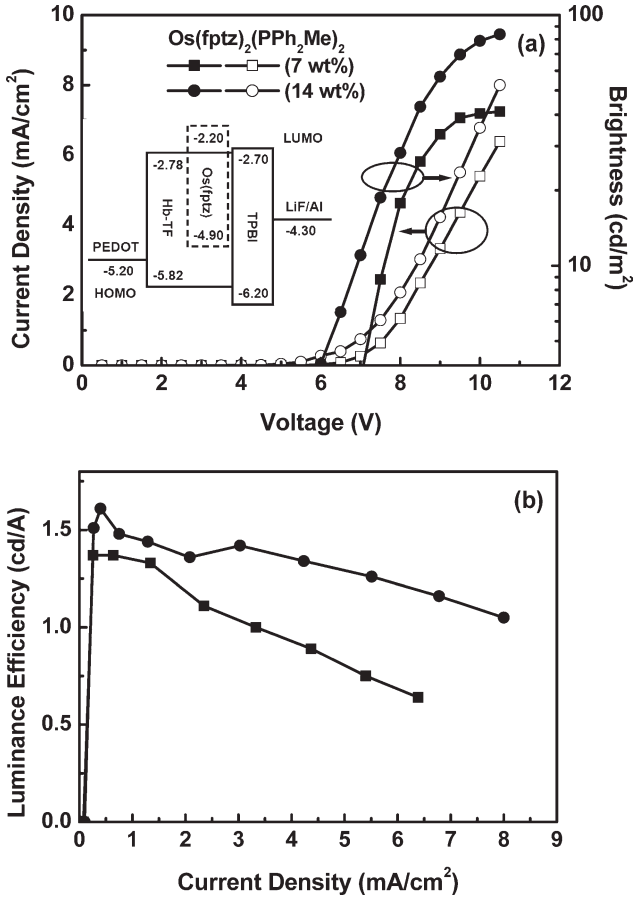


**FIGURE 7** (a) Current density and brightness versus voltage characteristics and (b) luminance efficiency versus current density characteristics of the devices based on the configuration of ITO/PEDOT:PSS/**Hb-TF**:*X* wt % $Os(fptz)_2(PPh_2Me_2)_2$/TPBI/LiF/Al. ($X = 7$ and 14). The inset is the energy level diagram for the $Os(fptz)_2(PPh_2Me_2)_2$-doped devices.

efficiency of the two devices are 1.37 and 1.61 cd/A. The turn-on voltage of 7 and 14 wt % $Os(fptz)_2(PPh_2Me_2)_2$-doped devices are 6.6 and 5.6 V. Thus, increasing the dopant concentration not only enhances the device performance of **Hb-TF**-based PLEDs but also decreases their turn-on voltage. The decrease of turn-on voltage suggests that the charges can be directly injected into the guest molecules at sufficiently high doping concentration; consequently, the guest domain serves as extra transport channels for the charge carriers and reduces the turn-on voltage.[57–62] **Hb-TF** provides an good packing environment for the dispersed $Os(fptz)_2(PPh_2Me_2)_2$ emitters and improves the device efficiency as a result of the reductions in the degrees of both triplet–triplet annihilation and self-quenching of the $Os(fptz)_2(PPh_2Me_2)_2$ guest.[63] Hence, the results demonstrate the potential of **Hb-TF** as a good polymeric host in the PLED applications.

**TABLE 5** Performances of the Devices Based on the Configuration of ITO/PEDOT:PSS/Hb-TF:*X* wt% $Os(fptz)_2(PPh_2Me_2)_2$/TPBI/LiF/Al

| Guest | $Os(fptz)_2(PPh_2Me_2)_2$ | |
|---|---|---|
| Dopant concentration (wt %) | 7 | 14 |
| Turn-on voltage (V)[a] | 6.6 | 5.6 |
| Max. Brightness (cd/m$^2$) | 41 @ 10.5 V | 84 @ 10.5 V |
| Max. L.E. (cd/A) | 1.37 | 1.61 |
| EL $\lambda_{max}$ (nm)[b] | 616 | 616 |
| CIE (*x*, *y*)[b] | (0.64, 0.36) | (0.64, 0.36) |

[a] Recorded at 1 cd/m$^2$.
[b] Recorded at 8 V.

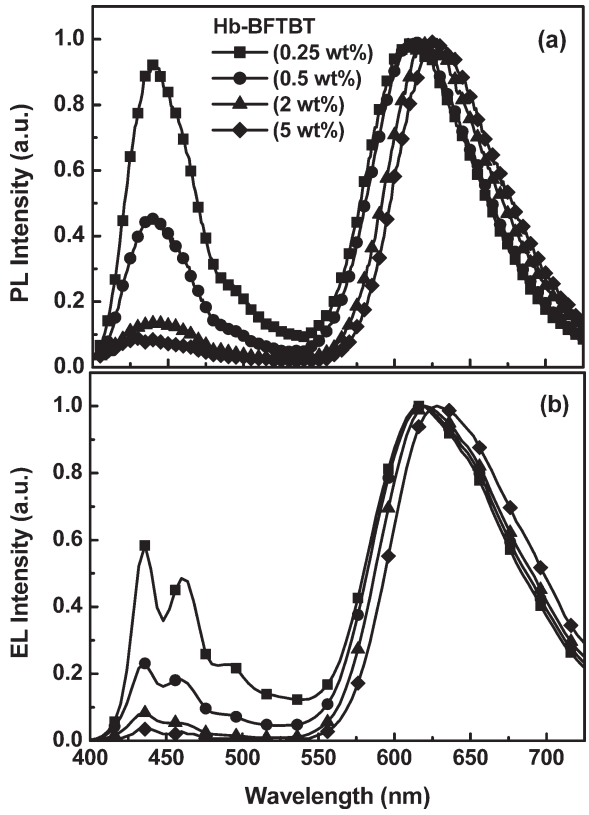


**FIGURE 8** (a) PL spectra and (b) EL spectra of the blends prepared from PFO as the host doped with the 0.25, 0.5, 2, and 5 wt % of **Hb-BFTBT** as the guest.

The PL and EL spectra of pristine **Hb-BFTBT** illustrate its potential as a red emitter. To further improve the device performance of **Hb-BFTBT**-based PLEDs, we used PFO as a host and **Hb-BFTBT** as the guest and fabricated double layer red PLEDs with the configuration of ITO/PEDOT:PSS (40 nm)/PFO:*X* wt % **Hb-BFTBT** (60–80 nm)/CsF (2 nm)/Al (100 nm). Figure 3 displays the PL spectrum of PFO in thin film. The emission band of PFO overlaps with the absorption band of the **Hb-BFTBT** thin film, suggesting efficient energy transfer from the PFO host to the **Hb-BFTBT** guest.[44,45] The PL and EL spectra of the PFO:**Hb-BFTBT** blends with **Hb-BFTBT** concentrations of 0.25–5 wt % are presented in Figure 8. The current density and brightness versus voltage characteristics of the devices are shown in Figure 9. Device performances are summarized in Table 6. As shown in Figure 8, both of the PL and EL spectra of the blends contain

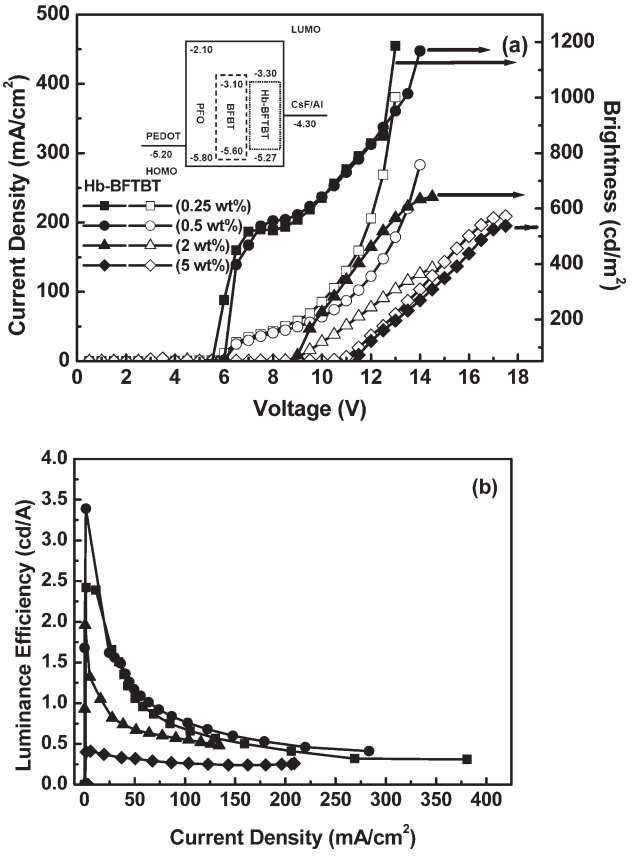


**FIGURE 9** (a) Current density and brightness versus voltage characteristics and (b) luminance efficiency versus current density characteristics of the devices based on the configuration of ITO/PEDOT:PSS/PFO:*X* wt % **Hb-BFTBT**/CsF/Al ($X = 0.25$, 0.5, 2, and 5). The inset is the energy level diagram for the **Hb-BFTBT**-doped devices.

two emission bands. The one with $\lambda_{max}$ at 440 nm, belongs to the characteristics emission of the PFO host, while the other one with $\lambda_{max}$ at 609 nm, belongs to the emission of the **HB-BFTBT** guest. The degree of energy transfer from the PFO host to the **Hb-BFTBT** guest increases as the doping concentration increases from 0.25 to 5 wt %.[53–55] At dopant concentration of 5 wt %, the host emission is almost extinct. According to the energy level diagram in inset of Figure 9(a), the $E_{HOMO}$ of **Hb-BFTBT** is 0.5 eV below the $E_{HOMO}$ of PFO. Therefore, holes can be effectively trapped in the **Hb-BFTBT** domains and allows efficient emission from the guest molecules.[56] The EL spectrum of the device using PFO:5 wt % **Hb-BFTBT** as a emitting layer shows saturated red emission with $\lambda_{max}$ at 638 nm and CIE coordinates at (0.63, 0.34). The maximum brightness and maximum luminance efficiency of the device are 538 cd/m$^2$ and 0.41 cd/A, which exhibited better performance than those of the pristine **Hb-BFTBT**-based PLEDs.[64] The turn-on voltage of the device is 10.1 V, which is higher than that of the pristine **Hb-BFTBT**. To further improve the performance of the device, inserting a hole-transporting layer or adding hole-transporting material into the PFO:**Hb-BFTBT** blend is now in progress in our group.

As shown in Figure 9 and Table 6, the device with the lowest **Hb-BFTBT** dopant concentration (0.25 wt %) show the best performance with turn-on voltage at 5.1 V, a maximum brightness of 1169 cd/m$^2$, and maximum luminance efficiency of 3.39 cd/A. The EL spectra of the device contain both blue ($\lambda_{max}$ at 440 nm) and red ($\lambda_{max}$ at 609 nm) emission bands with similar intensities [Fig. 8(a)]. The CIE coordinates of the device is at (0.53, 0.32). The incomplete energy transfer from PFO to **Hb-BFTBT** provides an opportunity of making white PLEDs via adding an auxiliary green dopant. For this purpose, an efficient green emitter, BFBT was added into the PFO:**Hb-BFTBT** blend.[46] White PLEDs with the double-layer configuration of ITO/PEDOT:PSS (40 nm)/PFO:*X* wt % BFBT:*Y* wt % **Hb-BFTBT** (60–80 nm)/CsF (2 nm)/Al (100 nm) were fabricated. Several concentrations of BFBT:**Hb-BFTBT** were attempted to achieve the ideal white light emission. The performances of the devices are summarized in Table 7. The current density and brightness versus voltage characteristics and the luminance efficiency versus current density curves of the devices are shown in Figure 10. The inset of Figure 10(a) shows the EL spectra of the devices at an applied potential of 6 V. At dopant concentrations of 0.05, 0.08, and 0.1 wt % for both BFBT and **Hb-BFTBT**, the devices have a maximum brightness of 1183, 1185, and 1886 cd/m$^2$ and maximum luminance

**TABLE 6** Performances of the Devices Based on the Configuration of ITO/PEDOT:PSS/PFO:*X* wt% Hb-BFTBT/CsF/Al

| Guest | Hb-BFTBT | | | |
|---|---|---|---|---|
| Dopant concentration (wt %) | 0.25 | 0.5 | 2 | 5 |
| Turn-on voltage (V)[a] | 5.0 | 5.1 | 7.7 | 10.1 |
| Brightness (cd/m$^2$)[b] | 369 | 329 | 188 | 74 |
| L.E. (cd/A)[b] | 1.99 | 1.97 | 0.97 | 0.37 |
| Max. Brightness (cd/m$^2$) | 1,187 | 1,169 | 643 | 538 |
| Max. L.E. (cd/A) | 2.42 | 3.39 | 1.96 | 0.41 |
| EL[c] | 616 | 620 | 620 | 638 |
| CIE (*x*, *y*)[c] | (0.45, 0.29) | (0.53, 0.32) | (0.60, 0.34) | (0.63, 0.34) |

[a] Recorded at 1 cd/m$^2$.
[b] Recorded at 20 mA/cm$^2$.
[c] Recorded at 11 V.

**TABLE 7** Performances of the Devices Based on the Configuration of ITO/PEDOT:PSS/PFO:*X* wt % BFBT:*Y* wt % Hb-BFTBT/CsF/Al

| Guest | BFBT:Hb-BFTBT | | | |
|---|---|---|---|---|
| Dopant concentration (wt %) | 0.05:0.05 | 0.08:0.08 | 0.1:0.1 | 0.25:0.25 |
| Turn-on voltage (V)[a] | 3.5 | 3.5 | 3.5 | 3.5 |
| Brightness (cd/m$^2$)[b] | 547 | 648 | 645 | 445 |
| L.E. (cd/A)[b] | 2.82 | 3.26 | 3.27 | 2.24 |
| Max. Brightness (cd/m$^2$) | 1,183 | 1,185 | 1,886 | 1,037 |
| Max. L.E. (cd/A) | 3.7 | 4.98 | 3.71 | 3.1 |
| CIE (*x*, *y*)[c] | (0.31, 0.34) | (0.33, 0.37) | (0.35, 0.38) | (0.42, 0.40) |

[a] Recorded at 1 cd/m$^2$.
[b] Recorded at 20 mA/cm$^2$.
[c] Recorded at 6 V.

efficiency of 3.70, 4.98, and 3.71 cd/A. Their CIE coordinates are (0.31, 0.34), (0.33, 0.37), and (0.35, 0.38), which are all very close to the CIE coordinates of the ideal white light, (0.33, 0.33). The turn-on voltages of all the devices are 3.5 V. Further increase of the dopant concentration to 0.25 wt % lowered the device performance, deviated the EL of the device from white emission. These results demonstrated the potential of **Hb-BFTBT** as a red emitter, and as a component in the applications of white PLEDs.

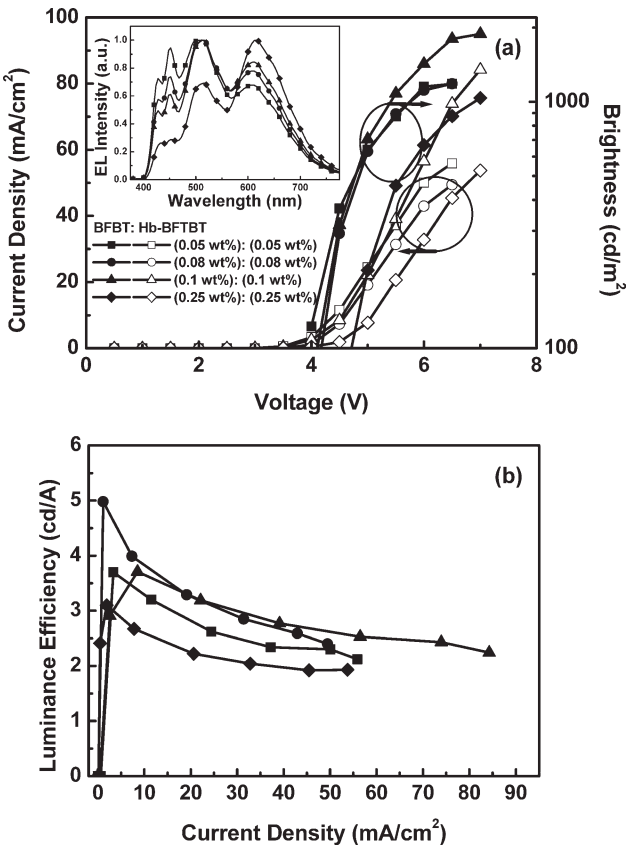


**FIGURE 10** (a) Current density and brightness versus voltage characteristics and (b) luminance efficiency versus current density characteristics of the devices based on the configuration of ITO/PEDOT:PSS/PFO:*X* wt % BFBT:*Y* wt % **Hb-BFTBT**/CsF/Al (*X* = 0.05, 0.08, 0.1, and 0.25, *Y* = 0.05, 0.08, 0.1, and 0.25). The inset is the EL spectra of the PFO-based devices codoped with BFBT and **Hb-BFTBT** at an applied potential of 6 V.

## CONCLUSIONS

In summary, to achieve good control in the color stability of solution-processable light-emitting materials, we developed a facile approach to synthesize diyne-functionalized **TF**, **BFBT**, and **BFTBT** as the blue, green, and red monomeric chromophores and prepared the corresponding blue, green, and red emitting Hb-Ps, **Hb-TF**, **Hb-BFBT**, and **Hb-BFTBT** through the [2+2+2] polycyclotrimerization. All the synthesized Hb-Ps show excellent thermal stability, moderate to high $T_g$s, and can be fabricated into the active layers of PLEDs based on the solution process. PL and EL spectra of the Hb-Ps clearly demonstrate that **Hb-TF**, **Hb-BFBT**, and **Hb-BFTBT** are blue-green, green, and red emitting materials. Because of its large $E_g$, **Hb-TF** was further evaluated as a polymeric host material. Saturated red electrophosphorescent devices with CIE coordinates of (0.64, 0.36), turn-on voltage (5.6 V) with a maximum luminance efficiency of 1.61 cd/A, and maximum brightness of 84 cd/m$^2$ were obtained when a **Hb-TF** was used as a host material doped with $Os(fptz)_2(PPh_2Me_2)_2$ as a guest material. The device efficiency of the red emitter, **Hb-BFTBT**, was further improved in a host–guest doped system by using **Hb-BFTBT** as red-emitting guest in the PFO host layer. Furthermore, a series of efficient white PLEDs were prepared by using **BFBT**, as auxiliary green dopant in the PFO:**Hb-BFTBT** blend. White PLEDs with CIE coordinates of (0.33, 0.37), which is close to that of ideal white light (0.33, 0.33), low turn-on voltage (3.5 V) with highest luminance efficiency of 4.98 cd/A, and maximum brightness of 1185 cd/m$^2$ were also achieved.

The authors thank the National Science Council and Ministry of Education for financial support.

## REFERENCES AND NOTES

**1** Burroughes, J. H.; Bradley, D. D. C.; Brown, A. R.; Marks, R. N.; Mackay, K.; Friend, R. H.; Burn, P. L.; Holmes, A. B. *Nature* **1990,** *347*, 539–541.

**2** Tasch, S.; List, E. J. E.; Ekström, O.; Graupner, W.; Leising, G.; Schlichting, P.; Rohr, U.; Geerts, Y.; Scherf, U.; Müllen, K. *Appl. Phys. Lett.* **1997,** *71*, 2883–2885.

**3** Yang, S. H.; Hsu, C. S. *J. Polym. Sci. Polym. Chem.* **2009,** *47*, 2713–2733.

**4** Müler, C. D.; Falcou, A.; Reckefuss, N.; Rojahn, M.; Wiederhirn, V.; Rudati, P.; Frohne, H.; Nuyken, O.; Becker, H.; Meerholz, K. *Nature* **2003,** *421*, 829–833.

**5** Pei, Q.; Yang, Y. *J. Am. Chem. Soc.* **1996,** *118*, 7416–7417.

**6** Virgili, T.; Lidzey, D. G.; Bradley, D. D. C. *Adv. Mater.* **2000,** *12*, 58–62.

**7** Leclerc, M. *J. Polym. Sci. Part A: Polym. Chem.* **2001,** *39*, 2867–2873.

**8** Scherf, U.; List, E. J. W. *Adv. Mater.* **2002,** *14*, 477–487.

**9** Li, J.; Bo, Z. S. *Macromolecules* **2004,** *37*, 2013–2015.

**10** Herguth, P.; Jiang, X.; Liu, M. S.; Jen, A. K. Y. *Macromolecules* **2002,** *35*, 6094–6100.

**11** Hou, Q.; Xu, Y.; Yang, W.; Yuan, M.; Peng, J.; Cao, Y. *J. Mater. Chem.* **2002,** *12*, 2887–2892.

**12** Chuang, C. Y.; Shih, P. I.; Chien, C. H.; Wu, F. I.; Shu, C. F. *Macromolecules* **2007,** *40*, 247–252.

**13** Geng, Y.; Trajkovska, A.; Katsis, D.; Ou, J. J.; Culligan, S. W.; Chen, S. H. *J. Am. Chem. Soc.* **2002,** *124*, 8337–8347.

**14** Wong, K. T.; Chien, Y. Y.; Chen, R. T.; Wang, C. F.; Lin, Y. T.; Chiang, H. H.; Hsieh, P. Y.; Wu, C. C.; Chou, C. H.; Su, Y. O.; Lee, G. H.; Peng, S. M. *J. Am. Chem. Soc.* **2002,** *124*, 11576–11577.

**15** Wu, C. C.; Liu, T. L.; Hung, W. Y.; Lin, Y. T.; Wong, K. T.; Chen, R. T.; Chen, Y. M.; Chien, Y. Y. *J. Am. Chem. Soc.* **2003,** *125*, 3710–3711.

**16** Wu, C. C.; Liu, W. G.; Hung, W. Y.; Liu, T. H.; Lin, Y. T.; Lin, H. W.; Wong, K. T.; Chien, Y. Y.; Chen, R. T.; Hung, T. H.; Chao, T. C.; Chen, Y. M. *Appl. Phys. Lett.* **2005,** *87*, 052103-1–052103-3.

**17** Ku, S. Y.; Chi, L. C.; Hung, W. Y.; Yang, S. W.; Tsai, T. C.; Wong, K. T.; Chen, Y. H.; Wu, C. I. *J. Mater. Chem.* **2009,** *19*, 773–780.

**18** Geng, Y.; Chen, A. C. A.; Ou, J. J.; Chen, S. A.; Klubek, K.; Vaeth, K. M.; Tang, C. W. *Chem. Mater.* **2003,** *15*, 4352–4360.

**19** Patten, T. E.; Matyjaszewski, K. *Adv. Mater.* **1998,** *10*, 901–915.

**20** Voit, B. *J. Polym. Sci. Part A: Polym. Chem.* **2000,** *38*, 2505–2525.

**21** Jikei, M.; Kakimoto, M. *Prog. Polym. Sci.* **2001,** *26*, 1233–1285.

**22** Tomalia, D. A.; Fréchet, J. M. *J. Polym. Sci. Part A: Polym. Chem.* **2002,** *40*, 2719–2728.

**23** Gao, C.; Yan, D. *Prog. Polym. Sci.* **2004,** *29*, 183–275.

**24** Haussler, M.; Tang, B. Z. *Adv. Polym. Sci.* **2007,** *209*, 1–58.

**25** Liu, J.; Lam, J. W. Y.; Tang, B. Z. *Chem. Rev.* **2009,** *109*, 5799–5867.

**26** Rosen, B. M.; Wilson, C. J.; Wilson, D. A.; Peterca, M.; Imam, M. R.; Percec, V. *Chem. Rev.* **2009,** *109*, 6275–6540.

**27** Voit, B. I.; Lederer, A. *Chem. Rev.* **2009,** *109*, 5924–5973.

**28** Maclachlam, M. J.; Ginzburg, M.; Coombs, N.; Raju, N. P.; Greedan, J. E.; Ozin, G. A.; Manners, I. *J. Am. Chem. Soc.* **2000,** *122*, 3878–3891.

**29** Yates, C. R.; Hayes, W. *Eur. Polym. J.* **2004,** *40*, 1257–1281.

**30** Wong, W. Y.; Liu, L.; Poon, S. Y.; Choi, K. H.; Cheah, K. W.; Shi, J. X. *Macromolecules* **2004,** *37*, 4496–4504.

**31** Hinderling, C.; Keles, Y.; Stockli, T.; Knapp, H. F.; delos Across, T.; Oelhafen, P.; Korczagin, I.; Hempenius, M. A.; Vancso, G. J.; Pugin, R.; Heinzelmann, H. *Adv. Mater.* **2004,** *16*, 876–879.

**32** Voit, B. *J. Polym. Sci. Part A: Polym. Chem.* **2005,** *43*, 2679–2699.

**33** Gregson, C. K. A.; Gibson, V. C.; Long, N. J.; Marshall, E. L.; Oxford, P. J.; White, A. J. P. *J. Am. Chem. Soc.* **2006,** *128*, 7410–7411.

**34** Liu, J.; Zhang, L.; Lam, J. W. Y.; Jim, C. K. W.; Yue, Y.; Deng, R.; Hong, Y.; Qin, A.; Sung, H. H. Y.; Williams, I. D.; Jia, G.; Tang, B. Z. *Macromolecules* **2009,** *42*, 7367–7378.

**35** Xu, K.; Peng, H.; Sun, Q.; Dong, Y.; Salhi, F.; Luo, J.; Chen, J.; Huang, Y.; Zhang, D.; Xu, Z.; Tang, B. Z. *Macromolecules* **2002,** *35*, 5821–5834.

**36** Peng, H.; Cheng, L.; Luo, J.; Xu, K.; Sun, Q.; Dong, Y.; Salhi, F.; Lee, P. P. S.; Chen, J; Tang, B. Z. *Macromolecules* **2002,** *35*, 5349–5351.

**37** Zheng, R. H.; Dong, H. C.; Peng, H.; Lam, J. W. Y.; Tang, B. Z. *Macromolecules* **2004,** *37*, 5196–5210.

**38** Chen, J.; Peng, H.; Law, C. C. W.; Dong, Y.; Lam, J. W. Y.; Williams, I. D.; Tang, B. Z. *Macromolecules* **2003,** *36*, 4319–4327.

**39** Haussler, M.; Qin, A.; Tang, B. Z. *Polymer* **2007,** *48*, 6181–6204.

**40** Liu, J. Z.; Zheng, R. H.; Tang, Y. H.; Haussler, M.; Lam, J. W. Y.; Qin, A.; Ye, M. X.; Hung, Y. N.; Gao, P.; Tang, B. Z. *Macromolecoles* **2007,** *40*, 7473–7486.

**41** Jim, C. K. W.; Qin, A.; Lam. J. W. Y.; Haussler, M.; Liu, J.; Yuen, M. M. F.; Kim, J. K.; Ng, K. M.; Tang, B. Z. *Macromolecules* **2009,** *42*, 4099–4109.

**42** Liu, J.; Zhong, Y.; Lam, J. W. Y.; Lu, P.; Hong, Y.; Yu, Y.; Yue, Y.; Faisal, M.; Sung, H. H. Y.; Williams, I. D.; Wong, K. S.; Tang, B. Z. *Macromolecules* **2010,** *43*, 4921–4936.

**43** Wu, F. I.; Shih, P. I.; Shu, C. F.; Tung, Y. L.; Chi, Y. *Macromolecules* **2005,** *38*, 9028–9036.

**44** Su, H. J.; Wu, F. I.; Shu, C. F. *Macromolecules* **2004,** *37*, 7197–7209.

**45** Huang, J. S.; Li, G.; Wu, E.; Xu, Q. F.; Yang, Y. *Adv. Mater.* **2006,** *18*, 114–117.

**46** Cheng, Y. J.; Liao, M. H.; Shih, H. M.; Shih, P. I.; Hsu, C. S. *Macromolecules* **2011,** *44*, 5968–5976.

**47** Malkina, A. G.; Brandsma, L.; Vasilevsky, S. F.; Trofimov, B. A. *Synthesis* **1996,** *1996,* 589–590.

**48** Tung, Y. L.; Lee, S. W.; Chi, Y.; Tao, Y. T.; Chien, C. H.; Cheng, Y. M.; Chou, P. T.; Peng, S. M.; Liu, C. S. *J. Mater. Chem.* **2005,** *15*, 460–464.

**49** Sonogashira, K.; Tohda, Y.; Hagihara, N. *Tetrahedron Lett.* **1975,** *50*, 4467–4470.

**50** Chen, C. H.; Cheng, Y. J.; Dubosc, M.; Hsieh, C. H.; Chu, C. C.; Hsu, C. S. *Chem. Asian J.* **2010,** *5*, 2483–2492.

**51** Cheng, Y. J.; Wu, J. S.; Shih, P. I.; Chang, C. Y.; Jwo, P. C.; Kao, W. S.; Hsu, C. S. *Chem. Mater.* **2011,** *23*, 2361–2369.

**52** Colombo, M. G.; Hauser, A.; Güdel, H. *Top. Curr. Chem.* **1994,** *171*, 144–171.

**53** Uchida, M.; Adachi, C.; Koyama, T.; Taniguchi, Y. *J Appl. Phys.* **1999,** *86*, 1680–1687.

**54** Chen, F. C.; Chang, S. C.; He, G.; Pyo, S.; Yang, Y.; Kurotaki, M.; Kido, J. *J. Polym. Sci. Part B: Polym. Phys.* **2003,** *41*, 2681–2690.

**55** Yeh, H. C.; Chein, C. H.; Shih, P. I.; Yuan, M. C.; Shu, C. F. *Macromolecules* **2008,** *41*, 3801–3807.

**56** Wu, F. I.; Shih, P. I.; Tseng, Y. H.; Chen, G. Y.; Chien, C. H.; Shu, C. F.; Tung, Y. L.; Chi, Y.; Jen, A. K. Y. *J. Phys. Chem. B* **2005,** *109*, 14000–14005.

**57** Adachi, C.; Baldo, M. A.; Thompson, M. E.; Forrest, S. R. *J. Appl. Phys.* **2001,** *90*, 5048–5051.

**58** Noh, Y. Y.; Lee, C. L.; Kim, J. J. *J. Chem. Phys.* **2003,** *118*, 2853–2864.

**59** Holmes, R. J.; D'Andrade, B. W.; Forrest, S. R.; Ren, X.; Li, J.; Thompson, M. E. *Appl. Phys. Lett.* **2003,** *83*, 3818–3820.

**60** Tung, Y. L.; Lee, S. W.; Chi, Y.; Chen, L. S.; Shu, C. F.; Wu, F. I.; Carty, A. J.; Chou, P. T.; Peng, S. M.; Lee, G. H. *Adv. Mater.* **2005,** *17*, 1059–1064.

**61** Tung, Y. L.; Chen, L. S.; Chi, Y.; Chou, P. T.; Cheng, Y. M.; Li, E. Y.; Lee, G. H.; Shu, C. F.; Wu, F. I.; Carty, A. J.; Peng, S. M.; Lee, G. H. *Adv. Funct. Mater.* **2006,** *16*, 1615–1626.

**62** Wu, C. H.; Shih, P. I.; Shu, C. F.; Chi, Y. *Appl. Phys. Lett.* **2008,** *92*, 233303-1–233303-3.

**63** Tsai, M. H.; Lin, H. W.; Su, H. C.; Ke, T. H.; Wu, C. C.; Fang, F. C.; Liao, Y. L.; Wong, K. T.; Wu, C. I. *Adv. Mater.* **2006,** *18*, 1216–1220.

**64** Virgili, T.; Lidzey, D. C.; Bradley, D. D. C. *Synth. Met.* **2000,** *111–112*, 203–206.